2011 American Control Conference
on O'Farrell Street, San Francisco, CA, USA
June 29 - July 01, 2011

Vision Based Iterative Learning Control of a MEMS Micropositioning Stage with Intersample Estimation and Adaptive Model Correction

Patrick J White and Douglas A. Bristow

Abstract—**In this work the use of an Iterative Learning Control (ILC) algorithm to precisely control a highly nonlinear Micro-Electro-Mechanical (MEMS) micropositioning stage is demonstrated. Vision-based feedback with low sampling rate is augmented with estimates from a Kalman Filter to generate a high sampling rate estimate of the output. Nonlinearities in the system are accounted for using a linear parameter varying model based on experimental results. An automatic model correction technique based on measurement residual is also presented that increases the final estimation accuracy by over 70 percent. The effectiveness of the approach is demonstrated by tracking a 4 Hz sinusoid using 10 Hz camera feedback with a resulting RMS error of 0.25 micrometers.**

I. Introduction

MICROPOSITIONG stages based on microelectro-mechanical system (MEMS) technology have shown significant potential for a number of complex applications. One of the fundamental challenges with MEMS development is the difficulty associated with obtaining fast, reliable displacement feedback. Unlike with macro-scale devices, MEMS are too small to be installed with current commercially available displacement sensors. Sensing must either be integrated into the mechanism during manufacture, or completely external to the device.

A number of on-chip MEMS sensing methods exist. Electrostatic capacitive sensing is capable of potentially high-precision, high-sensitivity displacement detection. Some stages that use electrostatic actuators can simply use a redundant actuator for sensing [1]. Simultaneous actuation and displacement sensing in a single electrostatic comb drive has also been shown [2]. Sensing can also be accomplished with material properties that change based on mechanical strain that occur during deflection or thermoelectric effects that occur during actuation. For instance, piezoresistivity has been used to track a mechanism's state [3]. It has also been proposed that certain devices can simply use the input signals for force and displacement control [4]. The fundamental problem with all of these methods is that they must be calibrated using a different sensing method before they can be employed. Furthermore the calibration might be dependent upon factors that change with time or cycles.

Vision based sensing is one of the simplest, and most versatile methods currently in use. The effort in setup and calibration is fairly small compared to other methods. Data such as displacement and vibrational magnitude can be obtained automatically with machine vision algorithms [5]. Furthermore multiple devices can be simultaneously observed with little or no additional effort. There are two major limitations of vision based control, however. First, slow camera frame rates limit the speed at which the system's response can be recorded. Second, real-time vision feedback requires complex software that runs at potentially a fraction of the camera's already slow frame rate.

Many MEMS applications such as high density data storage and fiber optical switching involve repetitive motion tasks. For such tasks an iterative learning algorithm can be used to accurately control the system in the absence of real-time feedback. However, slow vision feedback may lead to poor intersample behavior. This problem was addressed for a system with a higher error sampling rate than control frequency [6], though this is not the case for many MEMS devices. Another work demonstrated the use of a Kinematic Kalman Filter and ILC to control a single-axis macro scale mechanism with slow vision feedback [7], however this method cannot be directly applied to many MEMS due to the required linear model and fast acceleration measurement. The primary contribution of this work is to present an alternate method for implementing ILC with intersample estimation suitable for MEMS control, and demonstrate its effectiveness experimentally. This work also presents a novel technique for adaptively correcting the system gain due to modeling error.

II. System Design

The system chosen to demonstrate our ILC with intersample estimation is a MEMS positioning stage developed by the authors. It is a two degree-of-freedom R-θ manipulator. The stage was designed to be part of a high density array that will be used for precision coordinated manipulation tasks. Fig. 1 shows a picture of the fabricated prototype with significant features labeled.

The stage is a 50 μm thick monolithic mechanism manufactured using the silicon-on-insulator process found in [1]. The design requirements greatly influenced the decision to use thermal bimorph microactuators [8]. They offer both high force and high displacement properties in a very small

This work was supported by a University of Missouri Research Board grant.

P. J. White is with the Mechanical Engineering Department, Missouri University of Science and Technology, Rolla, MO 65401 USA

D. A. Bristow is with the Mechanical Engineering Department, Missouri University of Science and Technology, Rolla, MO 65401 USA (e-mail: dbristow@mst.edu).

package. There are a number of other advantages to the actuators. Unlike with electrostatic comb drives, they do not require high manufacturing precision. The thermal actuators are also fairly robust to environmental contamination which allows the stages to be operated outside of a cleanroom.

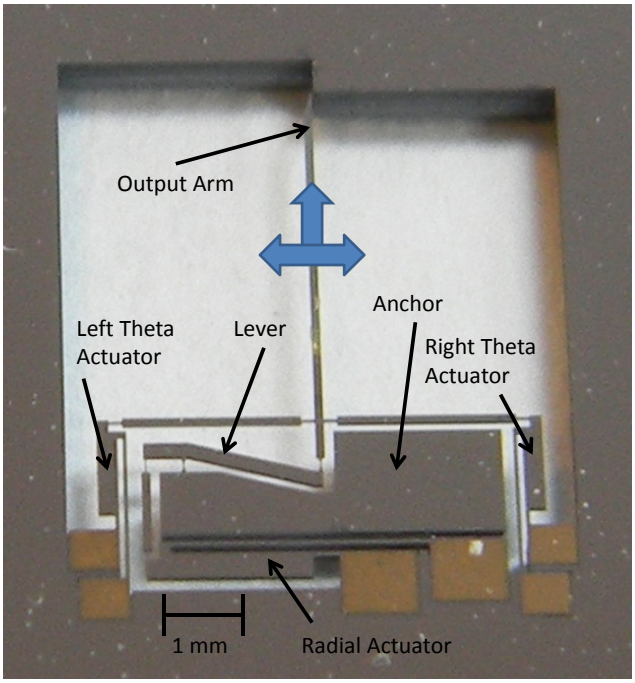

Fig. 1. The fabricated micromanipulation system. The thermal actuators and other significant features can be seen.

The shape of the actuators in the prototype stage was optimized for high force and small footprint. This was accomplished by increasing the hot arm to cold arm length ratio. The resultant high force output allowed for significant displacement amplification in the mechanism. The theta axis is linearly amplified by the long length of the output arm. The 2000 µm left and right theta actuators are antagonistically opposed. Besides allowing both directions of movement, it balances the device mechanically, and increases stiffness. Both factors decrease parasitic motion in unintended directions. A lever was used in the radial direction to amplify the displacement from the 3000 µm actuator. The center of flexure of the three pivots are in a line such that the displacement amplification is approximately linear in the displacement range of the device.

Testing was carried out on the radial axis of the prototype stage in air on a probe station with feedback recorded using a Pixelink PL-B741F camera mounted to an Infinitube system with a 20x objective. This system gives a resolution of about 0.35 µm. National Instruments *NI Vision Assistant* was used to automatically obtain displacement information from the video using a pattern matching algorithm.

III. Modeling

Accurate first-principles models of bimorph actuators are very difficult to develop because they demonstrate complex and highly nonlinear behavior due to surface heat loss by radiation and convection, intra-device heat transfer, and temperature dependent thermo-physical properties [9]-[10]. Here, standard system identification techniques are used to identify the system model. Swept sine input signals in the form $u(t) = A + 0.5\sin(\omega t)$, where A is the DC offset, were applied to the vertical actuation direction. Fig. 2 shows the results of the test. The prototype behaves like a first order system with a pole at 85 rad/s, however the DC gain of the system changes as the voltage increases. This is logical since the volumetric heat generation that drives the thermal actuators is proportional to the square of the input voltage.

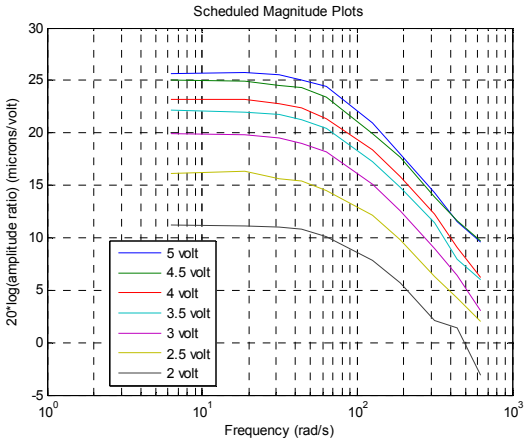

Fig. 2. Scheduled frequency response magnitude response plots showing that the gain increases with increase in offset, but the dynamics are constant

The system was modeled as a linear parameter varying first-order scalar system given by the differential equation

$$\tfrac{1}{85}\dot{x} + x = \beta g(u(t))u(t), \qquad (1)$$

where x is the vertical position of the system, $g(u(t))$ is the nonlinear gain and β is a correction factor that will be discussed in Section V. To identify $g(u(t))$ a gain curve was generated by giving the system a continuously increasing voltage input, and dividing the system output by the input voltage. Fig. 3 shows the results of 15 gain curve tests. Variation in the curves is due to contact resistance that changes with trial and contact pad location. The trail varying resistance change can be thought of as a wear parameter, and generally decreases with runs. Though the curve varies slightly, a clear trend can be seen. A 6th order curve fit derived from the average values of the 15 runs is given by

$$\begin{aligned} g(u(t)) = {} & -0.000144u(t)^6 + 0.00532u(t)^5 \\ & - 0.0634u(t)^4 + 0.268u(t)^3 + 0.00588u(t)^2 \\ & - 0.125u(t) + 0.0237 \end{aligned} \qquad (2)$$

Fig. 4 shows the displacement error that corresponds to the maximum difference between the gain fit and any of the individual curves. A correction method for this error will be presented in section IV.

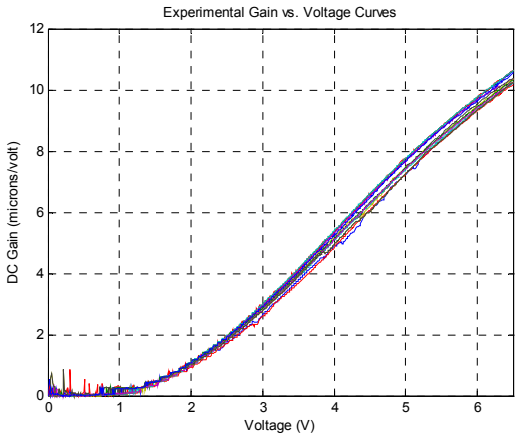

Fig. 3. 15 experimental gain curves run under different conditions. Some variation from one run to the next can be seen.

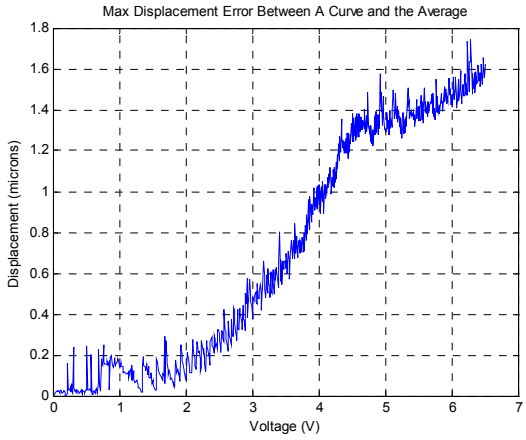

Fig. 4. This curve shows the maximum displacement error that occurs from using the average gain curve fit.

Section V presents a Kalman Filter that will be used to estimate the system output in between slow camera frames. This requires that the differential equation (1) be converted to the sampled state-space representation,

$$\begin{aligned} x(k+1) &= A_d x(k) + B_d v(k) \\ y(k) &= C_d x(k) \end{aligned} \tag{3}$$

where, $A_d = e^{-85dt}$, $B_d = \left(1 - e^{-85dt}\right)\beta$, $C_d = 1$, dt is the sample step size, and

$$v(k) = g\left(u(k)\right)u(k). \tag{4}$$

IV. Proportional ILC

Iterative Learning Control is a performance-enhancing feedforward control scheme for systems that repeat the same task or trajectory. Before the start of each iteration of the trajectory, the ILC algorithm uses the error signal from the previous iteration(s) to generate an updated feedforward control signal. ILC is an excellent choice for many MEMS systems for a number of reasons. MEMS are typically fully compliant, frictionless devices. The result is very repeatable behavior, which allows for extremely low error with the final control signal. This is because trial invariant disturbances such as modeling error is easily corrected with the algorithm, while trial varying disturbances such as measurement noise tend to be averaged out. Secondly, ILC typically runs off-line, which means slow vision processing techniques do not impair the effectiveness of the controller.

The prototype presented in this paper was modeled in Section III as a first order system, so a P-type algorithm [11] given by

$$u_{j+1}(k) = u_j(k) + \gamma e_j(k+1) \tag{5}$$

tracks the dynamics well. In (5), j is the ILC iteration, and k is the time step. The error signal is forward shifted by one time step in order to compensate for the usual one-step delay in the plant. γ is the proportional learning gain. Higher gains lead to faster correction, but are also more likely to cause divergence. For the system in question a learning gain of between 0.07 and 0.1 works well.

V. Intersample Estimation and Correction

In some cases slow feedback might not be enough information to control a system. In the case of an ILC control system, the error at measurement points might be very small, but the lack of control at intersample points might lead to large intersample error. In such cases a Kalman Filter is able to estimate the system between the measurement points and remove trial-varying measurement noise such that the ILC can correct for error accurately and at a higher rate than measurements are available.

A. Intersample Estimation

In order to apply the Kalman Filter [12], Assume a camera frame rate f_c, and an estimation frequency f_i, which should be chosen as the desired control frequency. Also assume f_i is a multiple of f_c. The camera multiplier, N, is f_i/f_c. The time step, dt is simply $1/f_i$. The system equations follow:

$$x(k+1) = A_d x(k) + B_d v(k) + w(k) \tag{6}$$

$$y(k) = C_d x(k) + r(k). \tag{7}$$

In these equations w is the modeling noise, r is the measurement noise, and $k=\{0,1,2,\ldots\}$. Note that for the experimental system the value of $v(k)$ during each time step is deterministic because the gain curve is assumed to be known. Initialize the Kalman Filter as per:

$$\hat{x}(0) = E[x(0)] \tag{8}$$

$$Z(0) = E[(x(0) - \hat{x}(0))(x(0) - \hat{x}(0))]. \tag{9}$$

For each time step, k, apply

$$\hat{x}(k+1 \mid k) = A_d \hat{x}(k \mid k) + B_d v(k) \tag{10}$$

$$M(k+1) = A_d Z(k) A_d^T + Q \tag{11}$$

to propagate to the next time step. In (11), Q is the modeling covariance which is based on the measurement noise. Depending on the time step one of two things comes next. If k is a multiple of N, correct the estimate with a measurement using:

$$F(k+1) = M(k+1)C_d^T \left[C_d M(k+1) C_d^T + R\right]^{-1} \tag{12}$$

$$\hat{x}(k+1 \mid k+1) = \hat{x}(k+1 \mid k) + F(k+1)\left[y_m(k+1) - C_d \hat{x}(k+1 \mid k)\right] \tag{13}$$

$$Z(k+1) = (I - F(k+1)C_d)M(k+1). \quad (14)$$

Where R is the measurement covariance. If k is not a multiple of N_s, use

$$\hat{x}(k+1|k+1) = \hat{x}(k+1|k) \quad (15)$$

$$Z(k+1) = M(k+1) \quad (16)$$

instead. Continue to propagate and update until an estimate at the final time step is obtained.

The Kalman Filter estimates the state at k using measurement data up to time k only. Since the ILC system runs after all measurements have been collected, it is possible to use a Kalman Smoother to use measurement information up the final time step, k_f to generate a more accurate estimate [7]. The estimate $\hat{x}(k|k_f)$ can be obtained using recursively using

$$S(k) = Z(k)A_k^T M(k+1)^{-1} \quad (18)$$

$$\hat{x}(k|k_f) = \hat{x}(k|k) + S(k)\left[\hat{x}(k+1|k_f) - \hat{x}(k+1|k)\right] \quad (19)$$

In these equations $k=\{k_f\text{-}1,k_f\text{-}2,\ldots,0\}$.

B. Estimation and Gain Correction

As seen in Fig. 4, there is some error associated with using an average gain curve. As previously discussed this is due to varying contact resistance. Because the estimator must propagate numerous times before updating with a measurement, small errors in the gain have a significant effect on the estimation accuracy. Since the error is approximately first-order, it can be corrected for using a modification factor on the input gain. The value of correction factor, β was determined using a numerical search algorithm based on the measurement residual. The residual is defined by

$$\tilde{y}(k) = y_m(k) - C_d\hat{x}(k|k-1). \quad (20)$$

The sign on the average residual indicates whether the estimator is underestimating or overestimating the system. For a set of data, an iterative numerical search given by

$$\beta_{n+1} = \beta_n + \alpha\frac{\tilde{y}_{n,ave}}{g(u_{n,ave})} \quad (21)$$

will find a value of β that reduces the average residual. In this equation α is the learning gain and n is the search iteration. The search algorithm is executed iteratively during each ILC iteration after collecting the output from the previous iteration and before generating a new input. The β search iteration index, n should not be confused with the ILC iteration index, j.

During the first ILC iteration (j=1), β_1=1. Otherwise β_1 is the final β from the previous ILC iteration. After collecting data the system is estimated with β_n. $\tilde{y}_{n,ave}$ and $u_{n,ave}$ can be calculated from the estimate. Afterward (21) is used to generate β_{n+1}. This process is repeated until the residual drops below a pre-defined value, or a maximum number of search iterations is reached. After the final estimation with the final correction factor, the ILC updates the control information for the next run.

The value of α in (21) is related to speed of convergence/divergence. A larger α may cause faster convergence, but also may cause divergence. This parameter can be tuned for better performance.

VI. Experimental Results

An ILC system requires that the timing of input and output signals is extremely accurate and repeatable. Triggering camera frames using the digital counter on the same DAQ board that is controlling the system allows for very precise timings. It was found that the camera used in the experiments was only able reliably trigger at 10 Hz with the maximum area of interest (AOI). As with many CMOS cameras it can run at higher frame rates with a decreased AOI. An AOI suitable for observing one device tip allows for a frame rate of up to 125 Hz. For this paper it is assumed that feedback is only available at 10 Hz, because this control method will be applied to an array of stages, which will require the full AOI to observe. However, since only one mechanism is being observed currently, measurements at 100 Hz are used in order to observe the intersample behavior. The 100 Hz measurements are only used for determining error and not used in the estimator, gain correction, or ILC.

A. ILC Tracking Without Intersample Estimation

10 Hz feedback with a proportional ILC is acceptable and accurate if the reference signal is slow enough that intersample dynamics are insignificant. An experiment was carried out to show that the system is able to accurately track a slowly changing reference. The reference used was a 4 second half-sinusoid with an amplitude of 30 µm. A learning gain of 0.1 was used in the ILC algorithm. Fig. 5 shows the system and output after 15 iterations. Fig. 6 shows that the RMS error decreases nearly monotonically with ILC iterations. The final RMS error calculated at 10 Hz was 0.40 µm, while the RMS error calculated at 100 Hz was 0.79 µm. The modest increase shows that intersample error is present, but is a fairly negligible effect. This behavior becomes more significant with a faster signal.

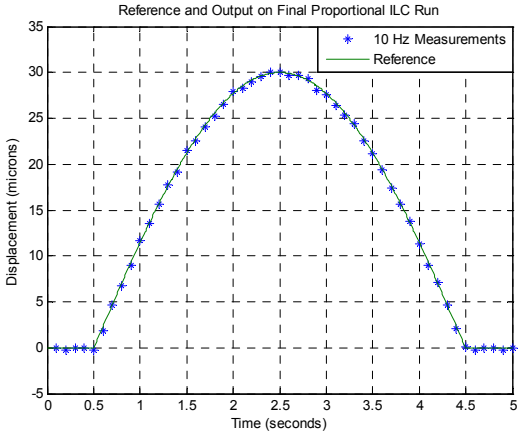

Fig. 5. ILC with 10 Hz feedback alone is able to track a slow half-sinusoid accurately with minimal intersample behavior.

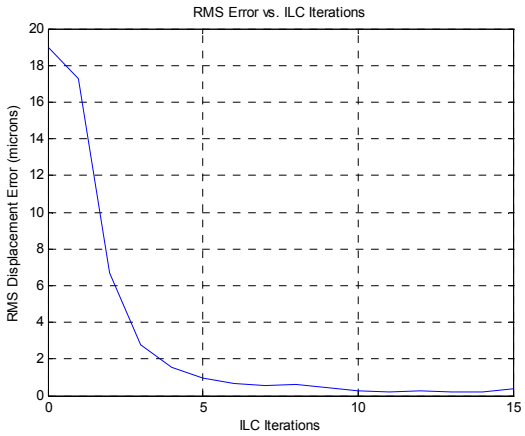

Fig.6. The RMS error of the system decreases sharply with ILC iterations.

Fig. 7 shows a 4 Hz offset sine wave that was used as a reference for the remaining tests. The same proportional ILC system was used to attempt to track the new reference. Fig. 8 shows the 10 Hz reference and the output of the system after 10 ILC iterations. The distortion in the reference due to slow measurements has caused very poor intersample behavior. Fig. 9 shows the error at 10 Hz and 100 Hz. The 10 Hz error is very low, signifying that the tracking near updates is good. However, intersample tracking is poor. The RMS error of 1.3 µm is primarily due to the first update point which is before control information is available. The 100 Hz RMS error, by contrast is 6.4 µm. Spikes of up to 13.8 µm are seen. It is obvious that proportional ILC alone is not sufficient to track this reference.

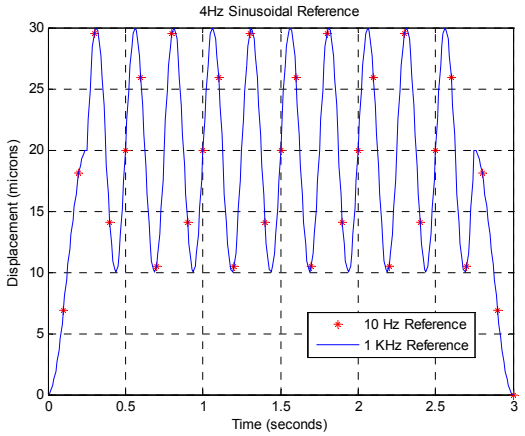

Fig. 7. The 4 Hz sinusoidal reference that will be used as a benchmark to compare the ILC controllers. Note the high degree of distortion at 10 Hz.

B. ILC Tracking With Intersample Estimation

Next the same reference is tracked using the estimator developed in Section V with and without gain correction. First, 15 iterations were run with intersample estimation and an ILC learning rate of 0.07 without gain correction. Fig. 10 shows the estimated and measured system. Overall the estimate is fairly good. The filter overestimates the output of the system at some of the peaks of the sine waves. Fig. 12 shows the total error between the system and the reference, as well as the error between only the estimator and the system. The total RMS error is 0.658 µm, and the RMS estimator error is 0.620 µm.

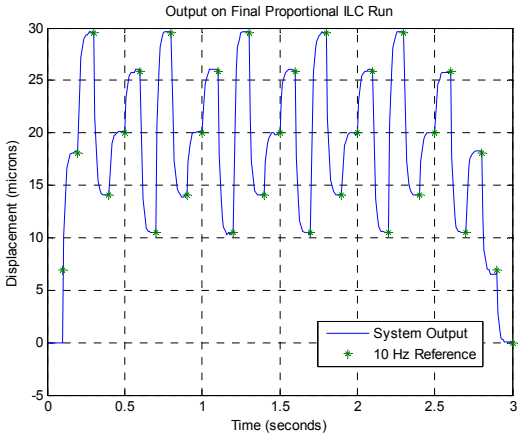

Fig. 8. The P-type ILC with 10 Hz feedback tracks the 4Hz signal poorly.

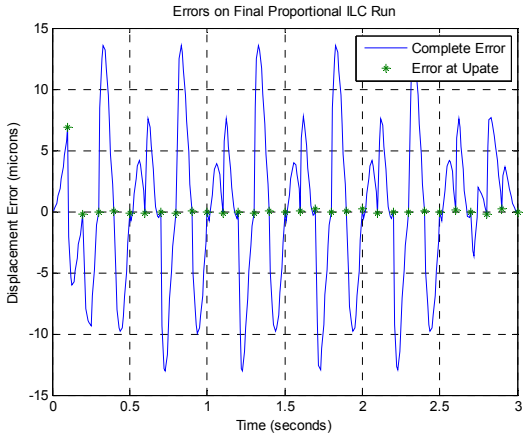

Fig. 9. Error graph for ILC without intersample estimation showing that error is very low at update points, but very high between updates.

Next a test was carried out with the same estimator and ILC algorithm, but with adaptive gain correction provided by (21). For each ILC iteration the numerical search for the modification factor was continued until the magnitude of the average residual was less than 0.005 µm. Fig. 11 shows the estimated and measured system. Very little deviation of the system from the estimate can be seen in this graph. Fig. 13 shows the shows the total error and estimator error. The total RMS error is 0.252 µm and the RMS estimator error is 0.176 µm. The effectiveness of the gain correction is apparent, as the RMS estimator error is improved by 72% and the total RMS error is improved by 61%. Fig. 13 shows that most of the error while tracking the sinusoid is due to estimator rather than the ILC. A more advanced model correction technique would likely improve the error even further.

VII. CONCLUSIONS

In this work a method for controlling a MEMS device using a combination of Iterative learning Control and a Kalman Filter is presented. The effectiveness of the estimator is demonstrated by tracking a fast sinusoidal reference with and without the estimator. A method for adaptive model correction is also presented that improves

the estimation accuracy by correcting the linear parameter varying model. Future work will include applying this control method to arrays of MEMS stages in order to perform precise coordinated motion tasks.

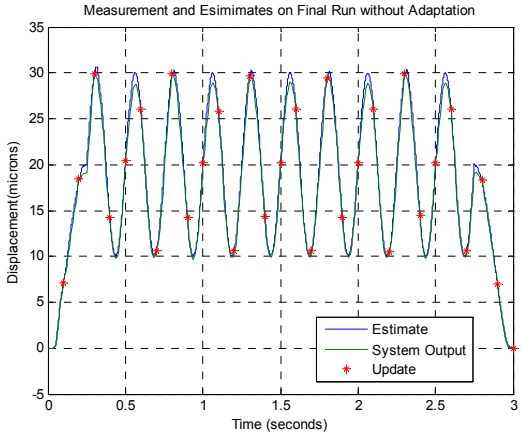

Fig. 10. The P-type ILC with intersample estimation and without adaptive gain correction. The filter overestimates some of the peaks.

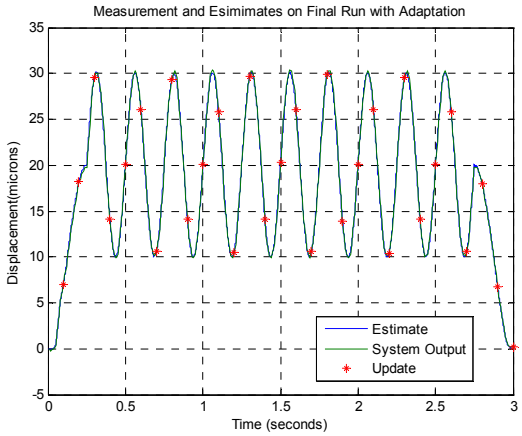

Fig. 11. The P-type ILC with intersample estimation and adaptive gain correction. Note the improved tracking.

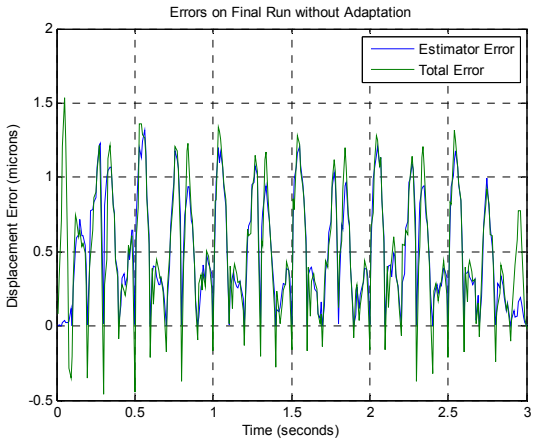

Fig. 12. The proportional ILC with intersample estimation and without adaptive gain correction.

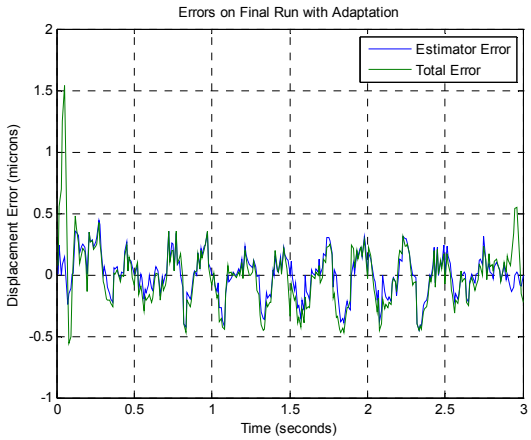

Fig. 13. The proportional ILC with intersample estimation and adaptive gain correction.

REFERENCES

[1] Mukhopadhyay, D., Dong, J., Ferreira, P.M., "Parallel Kinematic Mechanism based monolithic XY micro-positioning stage with rotary comb drive actuators," *Proc. of SPIE – The International Society for Optical Engineering*, 6882, art. No. 688209. ISBN:978-081947057-7, doi: 10.1117/12.762358.

[2] Dong, J., Ferreira, P.M., "Simultaneous actuation and displacement sensing for electrostatic drives," *J. of Micromechanics and Microengineering*, vol. 18, no. 3, March 2008, art. no. 035011.

[3] Anderson, J.K., Howell, L.L. Wittwer, J.W., and McLain, T.W., "Piezoresistive sensing of bistable micro mechanism state," *J. of Micromechanics and Microengineering*, vol. 16, no. 5, 2006, pp. 943-950.

[4] Waterfall, T.L., Teichert, K.B., and Jensen, B.D., "Simultaneous on-chip sensing and actuation using the thermomechanical in-plane microactuator," *J. of Microelectromechanical Systems*, vol. 17, no. 5, 2008, pp. 1204-1209.

[5] Zheng, D., Dagui, H., Zhang, D., and Wu, W, "An automatic MEMS testing system based on computer microvision," *2006 IEEE International Conference on Mechatronics and Automation, ICMA 2006*, art. no. 4026196, pp. 854-858.

[6] Oomen, T., Van De Wijdeven, J., and Bosgra, O., "Suppressing intersample behavior in iterative learning control," *Proc. of the IEEE Conference on Decision and Control*, art. no. 4738660, pp. 2391-2397.

[7] Wang, C.C., Tomizuka, M., "Iterative learning control of mechanical systems with slow sampling rate position measurements," *2008 Proc. of the ASME Dynamic Systems and Control Conference, DSCC 2008* (PART A), pp. 839-845.

[8] Guckel H., Klein J., Christenson T., Skrobis K., Laundon M., and Lovell E.G., "Thermo-magnetic metal flexure actuators," *Technical Digest- IEEE Solid-State Sensor and Actuator Workshop* , pp. 73-75

[9] Mankame, N.D., and Anathasuresh, G.K., "Comprehensive thermal modeling and characterization of an electro-thermal-compliant microactuator," *J. of Micromechanics and Microengineering*, vol. 11, no. 5, p. 452-462.

[10] Popa, D.O., Kang, B.H., When, J.T., Stephanau, H.E., Skidmore, G., and Geisberger, A. "Dynamic modeling and input shaping of thermal bimorph MEMS actuators," *Proc. IEEE International Conference on Robotics and Automation*, Vol. 1, pp. 1470-1475

[11] Bristow, D.A., M. Tharayil, and A.G. Alleyne, "A Survey of Iterative Learning Control," *IEEE Control Systems Magazine*, vol. 26, no. 8, pp. 1333-1336, 32001.

[12] Simon, D., *Optimal State Estimation*, Hoboken: Wiley-Interscience, 2006, pp. 128-129.